THE JOURNAL OF PHYSICAL CHEMISTRY C

Article

pubs.acs.org/JPCC

Ag−Cu Bimetallic Nanoparticles with Enhanced Resistance to Oxidation: A Combined Experimental and Theoretical Study

Na Rae Kim,[†] Kihyun Shin,[†] Inyu Jung,[†] Moonsub Shim,[†,‡] and Hyuck Mo Lee*[,†]

[†]Department of Materials Science and Engineering, KAIST, 291 Daehak-ro, Yuseong-gu, Daejeon 305-701, Republic of Korea

[‡]Department of Materials Science and Engineering and Frederick Seitz Materials Research Laboratory, University of Illinois, Urbana, Illinois 61801, United States

ABSTRACT: A simple oleylamine-based thermal decomposition process using different time steps for precursor injection was used to obtain bimetallic Ag−Cu nanoparticles with a narrow size distribution. Experimental and theoretical studies were carried out to demonstrate that these bimetallic nanoparticles are less prone to oxidation. The calculated energy trends for O_2 adsorption on the nanoparticles show that the adsorption energy declines rapidly when more than six O_2 molecules are present, indicating that O_2 is rarely adsorbed on Ag−Cu nanoparticles. Electron transfer from Cu to Ag within these bimetallic nanoparticles allows far better resistance to oxidation than monometallic Cu nanoparticles.

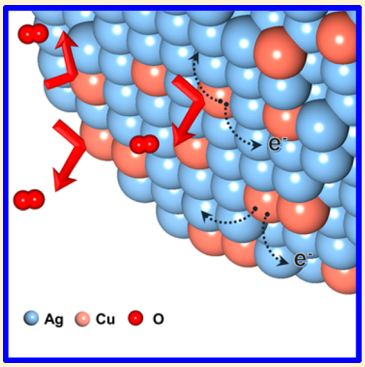

1. INTRODUCTION

Metallic nanoparticles possess many interesting electrical,[1] catalytic,[2,3] optical,[4] and magnetic properties[5] that have allowed them to be applied as metal electrodes with high conductivity and catalysts with enhanced activity.[6−8] Bimetallic nanoparticles provide a much broader space for engineering materials composition and structure/shape, leading to new and enhanced capabilities.[9−11] Bimetallic nanoparticles may also provide stability and functionality comparable to noble metals at a lower cost. For example, the high electrical conductivity and ease of processing of Ag nanoparticles are attractive qualities for electrodes and electrical interconnects.[1] However, the high cost of Ag is a hindrance to its use in actual commercial products. As an alternative, many researchers have investigated Cu nanoparticles, which are less expensive and exhibit comparably high electrical conductivity and catalytic activity.[6,12] However, Cu nanoparticles are easily oxidized; the development of approaches designed to mitigate oxidation, such as laser ablation, hydrogen reduction, and metal coating, have had limited success.[13,14] Bimetallic nanoparticles (i.e., Ag−Cu nanoparticles) may be a promising solution, but previous reports have indicated that they have unstable alloy or core−shell shapes.[13,15] Most chemical synthesis methods for nanoparticles are complicated or require an inert atmosphere. Moreover, toxic reducing agents are frequently used in nanoparticle synthesis.[16,17] Chen et al.[18] recently succeeded in synthesizing Ag−Cu nanoparticles with a stable core−shell shape. These nanoparticles were resistant to oxidation; however, their oxidation resistance could not be explained theoretically and was based entirely on experimental observations.[18] Furthermore, broad size distribution, easy aggregation, and the presence of nonbimetallic Ag-only particles resulting from this microwave-assisted synthesis can hinder characterization and may limit the applicability.[18] Here, we report a simple synthetic route to form stable Ag−Cu bimetallic nanoparticles that exhibit significantly improved resistance to oxidation compared to pure Cu nanoparticles. They have both Ag and Cu on the surface, and it poses a potential to be used as a nanocatalyst in oxygen reduction reaction.[12] Both experimental and theoretical approaches have been utilized to confirm the oxidation resistance of our Ag−Cu nanoparticles. Molecular dynamics (MD) and density functional theory (DFT) calculations, especially the adsorption energy trends with increasing numbers of O_2 molecules, verify the improved resistance to oxidation and provide insights on the mechanisms of charge transfer from Cu to Ag.

2. EXPERIMENTAL METHODS

2.1. Materials and Preparation of the Ag−Cu Nanoparticles. A modified thermal decomposition process was used to synthesize the Ag−Cu bimetallic nanoparticles. We used $AgNO_3$ (Sigma-Aldrich) as the Ag precursor, $Cu(acac)_2$ ($Cu(C_5H_7O_2)_2$, Sigma-Aldrich) as the Cu precursor, and oleylamine ($C_{18}H_{37}N$, Sigma-Aldrich) as the solvent, surfactant, and reducing agent.[19,20] All chemicals were used as received without further purification. For the synthesis of the bimetallic nanoparticles, 1.5335 g of $Cu(acac)_2$ was added to 90 mL of oleylamine in a three neck flask, which was then heated to 220 °C for 2 h while stirring. During this first reduction process, the Cu precursor thermally decomposed and was reduced by

Received: June 18, 2014
Revised: September 30, 2014
Published: October 17, 2014

oleylamine,[19] as indicated by the change in color of the solution from cobalt blue to dark red over time. After 2 h, the reaction mixture was cooled to 180 °C, and 1.5032 g of $AgNO_3$ was added to the solution. The reaction mixture was stirred at 180 °C for another 6 h prior to being cooled to room temperature to separate the nanoparticles. The nanoparticles were washed with methanol (CH_3OH, Sigma-Aldrich) and toluene ($C_6H_5CH_3$, ACS reagent ≥99.5%, Sigma-Aldrich) and separated by several centrifugation steps at 10 000 rpm for 40 min. The purified nanoparticles were then dried in a vacuum oven at 40 °C for more than 12 h. An ink-type suspension of Ag−Cu nanoparticles was prepared by dispersing the fully dried nanoparticles at 30 wt % in toluene and sonicating in a homogenizing bath.

Instrumentation and Characterization. Transmission electron microscopy (TEM) and high-resolution TEM (HRTEM) were carried out on a JEM-ARM200F (operated at 300 kV) and a field-emission Tecnai G2 F30 TEM (FEI company), respectively. Energy-dispersive X-ray spectroscopy (EDS) line scans were obtained using an aberration-corrected scanning transmission electron microscope (Cs-corrected transmission electron microscope, JEM-ARM200F; operated at 200 kV). X-ray diffraction (XRD) analysis was conducted using high power powder XRD (D/MAX-2500; RIGAKU). The oxidation state of the nanoparticles was obtained by X-ray photoelectron spectroscopy (XPS) (Sigma Probe; Thermo VG Scientific).

2.2. Computational Procedure. To derive reasonable simulation results, we performed a multiscale simulation approach. We performed MD simulations to optimize the most stable Ag−Cu bimetallic nanoparticle and DFT calculations to determine the O_2 adsorption energies.

In the MD simulations, we performed classical MD simulations with canonical ensemble conditions (NVT) as implemented in the XMD code[21] and used the quantum Sutton-Chen (Q-SC) many-body potential. The choice of this potential is appropriate to describe the nanoscale system under consideration because quantum effects and surface characteristics are considered.[22,23] The Q-SC many-body potential was reported by the Goddard group and has the same form as the SC potential.[22,24] This advanced potential includes quantum corrections to consider the zero-point energy and provides improved predictions of the temperature-dependent properties, which make it suitable for the calculation of various physical properties, such as defect, surface, interface, and vacancy formation energies in nanoscale systems.[22,25] To solve the Newton's dynamics equation, the fifth-order Gear predictor−corrector algorithm was utilized with a time step of 0.001 ps.[26] We carried out simulated annealing (SA) using a MD simulation to determine the most stable Ag−Cu nanoparticle. The simulation box is set to 1000 Å × 1000 Å × 1000 Å for the whole MD simulation.

In the DFT calculations, we performed GGA-level spin-polarized Kohn−Sham DFT calculations as implemented in the atomic orbital-based DMol^3 package.[27,28] The Kohn−Sham equation was expanded in a double-numerical quality basis set with polarization functions (DNP). The revised Perdew−Burke−Ernzerhof (RPBE) functional was employed to describe the exchange correlation energy.[29−32] This functional describes atomic or molecular binding to a transition metal well and is widely used.[33−36] The range for the orbital cutoff was set to 5.0 Å. The DFT semicore pseudopotential was chosen to treat the core electrons of the heavy Ag and Cu atoms.[37] In this study, the size of the Fermi smearing was 0.003 Ha (1 Ha = 27.2114 eV). The convergence tolerances for the energy, force, and displacement were 2×10^{-5} Ha, 0.004 Ha Å^{-1}, and 0.005 Å, respectively.

In order to compare O_2 adsorption properties, we prepared two nanoparticle systems (i.e., Cu and Ag−Cu bimetallic) composed of 55 atoms (diameter is approximately 1.0 nm). The structure of these nanoparticles was icosahedron (Ih), which is a well-known stable structure for this size.[38] The 55-atom Ih structure contained three layers, the first central layer of one atom, the second layer of 12 atoms, and the third layer of 42 atoms. The Ih structure of the Cu nanoparticle can be easily constructed because only one element is present. For the Ag−Cu bimetallic nanoparticle, we performed MD simulations and DFT calculations to determine the most reasonable structure and chemical ordering. There are many studies to find the most stable structure of Ag−Cu and Au−Cu bimetallic nanoparticles in various compositions and sizes by using the genetic algorithm[39−41] or Monte Carlo simulation.[42] These are famous and general methods to find the global minimum of a nanoparticle. However, in this study, the following three steps were used to find the structure of a Ag−Cu bimetallic nanoparticle that best represented experimentally obtained structures, which are certainly not the global minimum configuration but the metastable or local minimum configuration. The first step was the "nanoparticle generation" step that generates 12 random nanoparticles at 1000 K by changing the equilibration time from 200 to 2400 ps at an interval of 200 ps. The second step was the "nanoparticle cooling" step (i.e., the SA procedures) using the 12 nanoparticles generated by the first step. In the SA procedures, the 12 generated nanoparticles were cooled from 1000 to 300 K with a rate of 20 K per 600 ps (about 30 K ns^{-1}). The final step was the "nanoparticle optimization" step. In this step, we carried out geometry optimization with DFT calculations for the 12 stable nanoparticles produced by the second step. Finally, we determined the most stable Ag−Cu bimetallic nanoparticle of our interest by comparing the relative energy difference among the 12 bimetallic nanoparticles.

Using the Cu and Ag−Cu bimetallic nanoparticle systems, we calculated the O_2 adsorption energies by varying the number of adsorbed O_2 molecules (up to seven O_2 molecules were adsorbed on each nanoparticle). The adsorption energies (E_{ad}) were calculated using the following equation

$$E_{ad} = E_{nO_2+NP} - (E_{(n-1)O_2+NP} + E_{O_2})$$

where E_{nO_2+NP} is the energy of the entire system after n number of O_2 molecules have adsorbed, and E_{O_2} is the chemical potential of the O_2 molecules.

3. RESULTS AND DISCUSSION

3.1. Galvanic Displacement for the Preparation of Ag−Cu Bimetallic Nanoparticles. We used a modified thermal decomposition process to synthesize the monodisperse Ag−Cu bimetallic nanoparticles.[20,43] The key differences were the stepwise injection of precursors and the variation in temperature to separate the nucleation of Cu and the galvanic displacement. Cu^0 nanoclusters were first synthesized by adding $Cu(acac)_2$ to the reaction flask with 90 mL of oleylamine at 220 °C, as shown in Scheme 1. After several hours, the reaction mixture was cooled to 180 °C, and the Ag precursor (i.e., $AgNO_3$) was immediately added to the solution. The high Cu

dx.doi.org/10.1021/jp506069c | J. Phys. Chem. C 2014, 118, 26324−26331

Scheme 1. Schematic Representation of the Synthesis of Ag–Cu Nanoparticles[a]

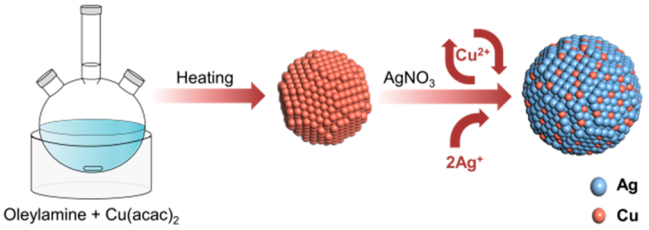

[a]Galvanic displacement and reduction of Cu occur due to the difference in Ag and Cu redox potentials and oleylamine-based thermal decomposition, respectively.

synthesis temperature and the lower Ag precursor addition temperature after the reduction of Cu were used for the following reasons. First, when Cu nanoparticles are synthesized at lower temperatures (i.e., lower than 180 °C), Cu (I, II) oxides are easily formed.[44] In addition, when the synthesis temperature is decreased, the growth process dominates instead of the nucleation process.[43] Therefore, we obtained more uniform nanoparticles by increasing the temperature. A lower Ag precursor addition temperature was used to minimize/eliminate growth during the galvanic displacement of Cu by Ag. When the Ag precursor chemically decomposes, electron transfer between Ag^+ and Cu^0 occurs. On the basis of the reduction potentials, Cu is more easily ionized than Ag (i.e., Cu^0 loses its electrons to the Ag ion leading to the coexistence of Ag and Cu in each nanoparticle). At the same time, reduction of the Cu ion occurs competitively for 6 h at 180 °C. As a result of these reactions, nanoparticles with randomly mixed but separate Ag and Cu domains are formed.

3.2. Ag–Cu Bimetallic Nanoparticles in the Mixed Structure. Figure 1a presents a TEM image and Figure 1b XRD results of the synthesized nanoparticles. The narrow size distribution of the synthesized nanoparticles can be readily seen. The XRD analysis was conducted with a fully dried powder of the nanoparticles. Uniform and spherical nanoparticles with a diameter of 13.9 nm ($\sigma \leq 7.6\%$, standard deviation) were obtained. The size distribution of the Ag–Cu nanoparticles was calculated using images obtained from the TEM analyses (an example shown in Figure 1a) where more than 100 nanoparticles were counted. The results show a highly controlled size compared to previous reports.[18] Figure 1c shows a HRTEM image of a nanoparticle. The observed lattice spacing values match the expected lattice parameters. Table 1 shows the lattice parameters obtained from XRD analysis (i.e., $d_{Ag(111)}$= 2.360 Å and $d_{Cu(111)}$= 2.090 Å), consistent with the HRTEM results. In addition, there were no obvious signs of an oxide layer surrounding the nanoparticle (a previous report

Table 1. XRD Data for Lattice Parameters

	peak position (2Θ) (degree)		lattice parameter (Å)	
	(111)	(200)	d_{111}	d_{200}
Ag	38.100	44.187	2.360	2.048
Cu	43.261	50.521	2.090	1.805

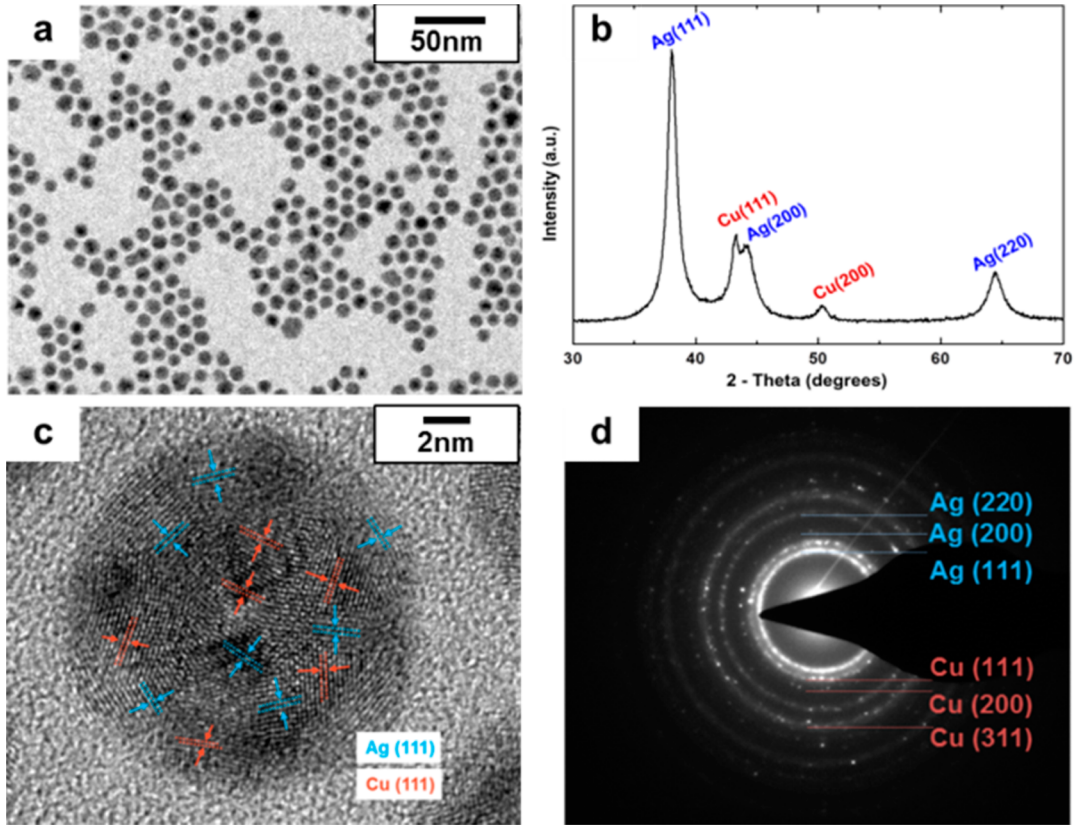

Figure 1. (a) TEM image of the Ag–Cu nanoparticles synthesized at 220 °C for 2 h (initial Cu nanoparticle nucleation and growth) and 180 °C for 6 h. (b) Characterization by XRD of the synthesized Ag–Cu nanoparticles. (c) HRTEM image of a nanoparticle. (d) SAED patterns of the Ag–Cu nanoparticles.

dx.doi.org/10.1021/jp506069c | J. Phys. Chem. C 2014, 118, 26324–26331

suggested that such oxide layers can be confirmed by HRTEM analysis).[45] Figure 1d shows the SAED pattern of a Ag−Cu bimetallic nanoparticle, indicating that the nanoparticle is polycrystalline.

Although the TEM, HRTEM, XRD, and SAED results are consistent, they are not sufficient to confirm the bimetallic shape of the Ag−Cu nanoparticle. Therefore, energy-dispersive X-ray spectroscopy (EDS) analysis, as shown in Figure 2, was also carried out. The line scan in Figure 2b shows that Ag and Cu are mixed well in the nanoparticle. The line scans from more than five samples all showed a similar distribution of Ag and Cu. The atomic ratio of Ag:Cu was 74.5:25.5% and was nearly constant within each particle.

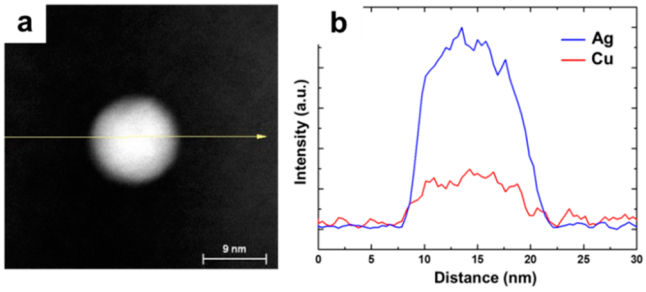

Figure 2. (a) TEM-EDS image of a Ag−Cu bimetallic nanoparticle synthesized at 220 °C for 2 h for initial Cu nanoparticle nucleation and growth and 180 °C for 6 h for the galvanic displacement and reduction to the bimetallic nanoparticle. (b) Line scan showing the distribution of Ag and Cu for a mixed structure along the direction denoted by the yellow line in (a).

On the other hand, the Cu−Ag core−shell nanoparticles have been synthesized using galvanic replacement.[10,13,15,46] Yang et al.[47] also fabricated the Ag−Au core−shell nanoparticle by strong reduction of the shell layer with suppressing galvanic replacement during the synthetic process. Furthermore, Gao et al.[48] conducted the surface-protected annealing process with SiO_2 to fabricate the fully alloyed Ag−Au nanospheres at the very high temperature. The difference in configuration seems to come from the use of a weak reducing agent, oleylamine, in this study.

3.3. Oxidation of Ag−Cu Bimetallic Nanoparticles. To confirm the crystallinity and the oxidation state of the Ag−Cu nanoparticles, XPS analysis was conducted. The results were compared to the results for pure Cu nanoparticles. For this purpose, the Cu nanoparticles were synthesized by the same thermal decomposition process in oleylamine without the galvanic displacement reaction. The XPS analysis also verified the ability of the Ag−Cu nanoparticles to resist oxidation. To conduct the XPS analysis, the synthesized bimetallic Ag−Cu and monometallic Cu nanoparticles were fully dried under vacuum for more than 10 h. Then the samples were prepared by putting powder of nanoparticles on carbon tape on a silicon wafer piece. The XPS measurements were conducted on Ag−Cu and Cu nanoparticles using the same preparation. Figure 3a,b presents the Cu $2p_{3/2}$ curves of the monometallic Cu nanoparticles and Ag−Cu bimetallic nanoparticles, respectively. In Figure 3a, two peaks at 932.3 and 934.0 eV, which are based on Gaussian curve fitting, can be observed. These peaks can be

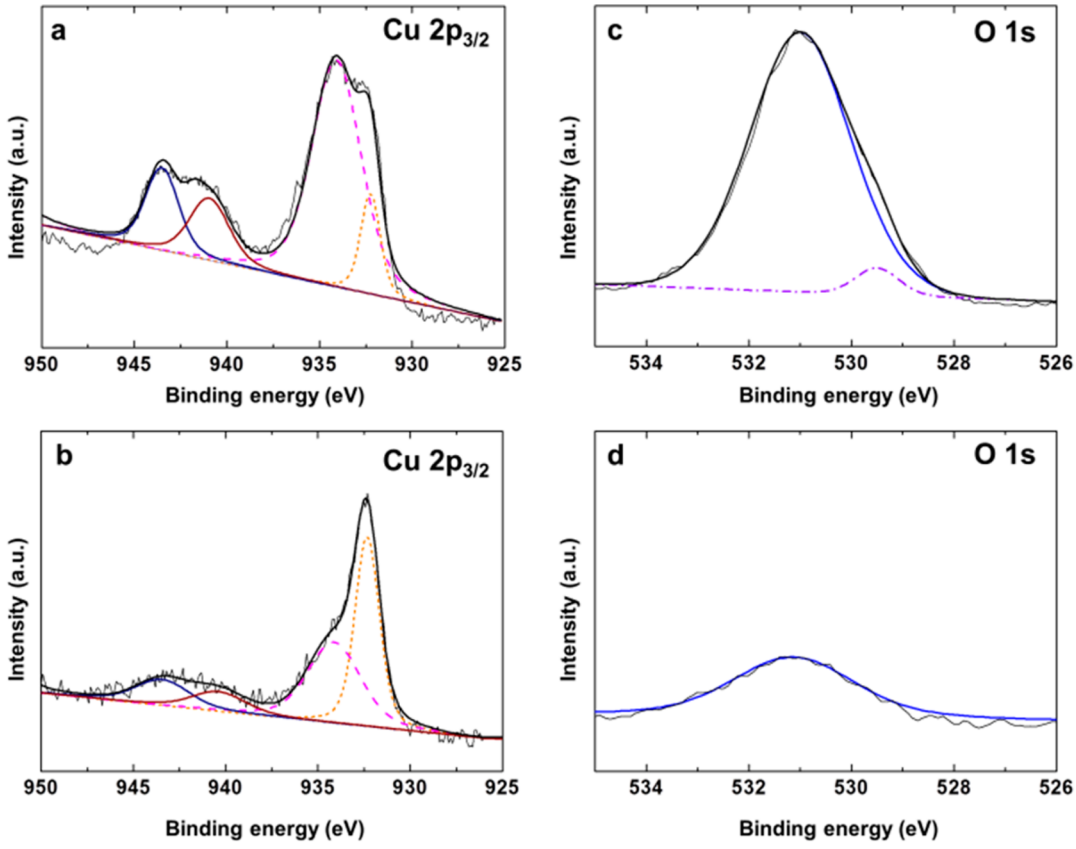

Figure 3. XPS spectra of the Cu 2p3/2 for the pure Cu nanoparticles synthesized at 220 °C for 6 h (a) and the Ag−Cu nanoparticles prepared at 220 °C for 2 h and 180 °C for 6 h (b). XPS O 1s regions of the Cu nanoparticles (c) and the Ag−Cu nanoparticles (d).

dx.doi.org/10.1021/jp506069c | J. Phys. Chem. C 2014, 118, 26324−26331

attributed to the zerovalent copper (Cu^0) and Cu^{2+} of CuO, respectively.[49,50] The existence of the oxide was confirmed by the presence of the oxygen peak at 529.5 eV. In the case of monometallic Cu nanoparticles, the atomic ratio of Cu^0:Cu^{2+} was 1:3.7, suggesting that Cu is easily oxidized without any intentional oxidation treatments. On the other hand, Figure 3b shows that Ag−Cu bimetallic nanoparticles exhibit better resistance to oxidation. The main peak at 932.2 eV is attributed to Cu^0, and the smaller peak at 934.1 eV corresponds to Cu^{2+}. Following the reported full-width-at-half-maximum value of the Cu $2p_{3/2}$ peak (3.4 eV for CuO), the broader peak at 934.1 eV can be assigned to CuO.[51] On the basis of the curve fitting results, the atomic ratio of Cu^0:Cu^{2+} was estimated to be 1:1, indicating the presence of significantly smaller amounts of CuO.

The O 1s peaks are typically observed between 528 and 535 eV in the XPS.[52] The lattice O is expected to exhibit a binding energy between 529.0 and 530.0 eV. Two peaks at 529.5 and 530.9 eV were observed in Figure 3c.[53] These two peaks can be attributed to the lattice O and the chemisorbed O_2 on the surface, respectively.[54] For the Ag−Cu, the intensity of O 1s is much lower, appearing at 530.4 eV to indicate the presence of Cu oxides.[55,56]

Although a small amount of O_2 can be chemisorbed on the surface, the above XPS result confirmed that the Ag−Cu bimetallic nanoparticles exhibit enhanced resistance to oxidation compared to the monometallic Cu nanoparticles. The amount of zerovalent Cu increased from 21.3% in the monometallic Cu nanoparticles to 49.3% in the Ag−Cu bimetallic nanoparticles. To support the finding of enhanced resistance to oxidation and gain insights on the reason for this enhancement, the adsorption energies of oxygen on the Ag−Cu bimetallic nanoparticles and pure Ag and Cu nanoparticles were calculated using DFT.

3.4. Optimization of the Ag−Cu Bimetallic Nanoparticles. As shown in Scheme 2, Cu and Ag−Cu bimetallic nanoparticles composed of 55 atoms in the optimized Ih structure were obtained from the MD simulations and DFT calculations. The optimization of the nanoparticle was carried out as follows. A 55-atom nanoparticle composed of 38 Ag atoms and 17 Cu atoms was first melted at 1000 K. The composition corresponds to approximately 31 at. % Cu, which is similar to the experimental value obtained for our nanoparticles. A total of 12 melted random nanoparticles were generated ("nanoparticle generation" step) by varying the optimization time and simulated annealing (SA) procedures ("nanoparticle cooling" step) to obtain a stable nanoparticle at room temperature. Finally, geometry optimization was carried out using DFT calculations ("nanoparticle optimization" step) to acquire more accurate energies for each nanoparticle. Details are given in the Computational Procedure section. The results are shown in Figure 4.

Scheme 2. Established Nanoparticle Systems Composed of 55 Atoms: (a) Cu (Orange) Nanoparticle with an Ih Structure and (b) Ag (Blue)−Cu Bimetallic Nanoparticle with an Ih Structure, Which Were Optimized Using MD Simulations and DFT Calculations[a]

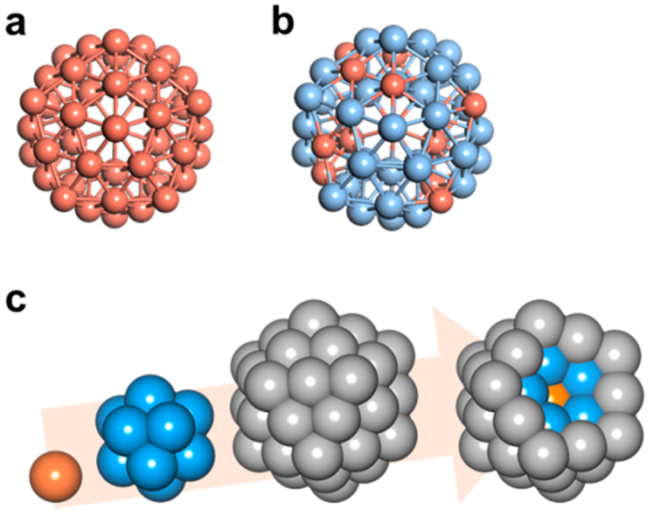

[a]The specific parts of the core and shell layer are shown in (c).

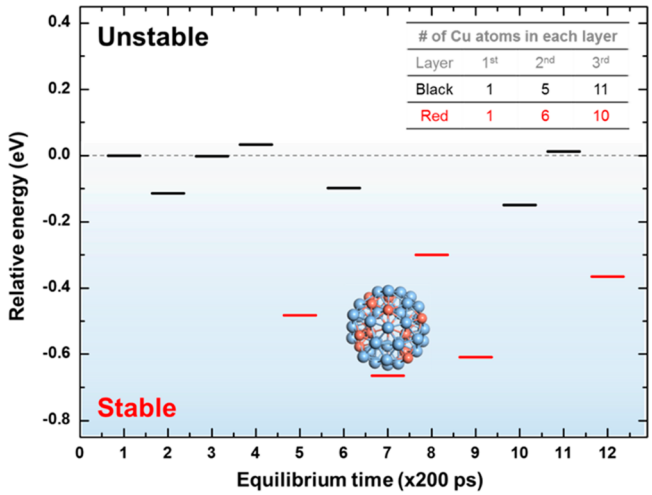

Figure 4. Relative energies of the 12 Ag−Cu bimetallic nanoparticles. There are two configurations due to a Cu position change represented by the black and red lines. The difference between black and red is the number of Cu atoms in the second and third layers. More Cu atoms are located on the surface for the black than for the red.

After the SA procedures ("nanoparticle cooling" step) were complete, the 12 stable nanoparticles were obtained at room temperature. At first, 10 nanoparticles were examined to choose stable nanoparticles with structures that were compatible to and as similar as possible with the experimentally synthesized ones. Two types were identified (black and red in the inset of Figure 4). The tenth configuration is less stable than the ninth one, and thus two more nanoparticles were simulated to confirm that this trend of two configuration types persisted. As a result, we conclude that even if we take more configurations into account we end up with two types identified as red and black. Every configuration after SA has the Ih structure because it is extremely stable when a nanoparticle is composed of a magic number (13, 55, and 147) of atoms.[57] As shown in Scheme 2c, there are three layers in the 55-atom icosahedral nanoparticle that include the core (first layer), subsurface (second layer), and surface (third layer). There are two types of nanoparticles based on the position of the Cu atoms. The major difference between the black and the red types in Figure 4 is the number of Cu atoms in the surface layer (i.e., the third layer). Either 11 (black) or 10 (red) Cu atoms are positioned in the third layer of each nanoparticle, and either 5 (black) or 6 (red) Cu atoms are located in the second layer of each nanoparticle. The only

dx.doi.org/10.1021/jp506069c | J. Phys. Chem. C 2014, 118, 26324−26331

distinguishable difference is the number of Cu atoms on the surface (third layer) for the states shown in black in Figure 4, which indicates that all of the structures in red are more stable. In general, the different surface energies of elements can determine the position of each element in a given system. An element with higher surface energy prefers to occupy the inner layer of a nanoparticle (first and second layers). The surface energy of Cu (1.77 J m^{-2}) is higher than that of Ag (1.32 J m^{-2}).[58] Therefore, one more Cu atom positioned in the third layer (configurations in black) would increase the total energy and result in the configurations in red being more stable. According to the surface energy argument, the Cu−Ag core−shell nanoparticle is the most stable among various structures. However, our experimental results indicate that our product of synthetic process is a randomly mixed one even though it may be energetically less stable. Thus, we simulated the Ag−Cu bimetallic nanoparticle having a randomly mixed configuration (approximately 31 at. % of Cu) by MD simulation.

3.5. Oxygen Adsorption Trend Based on Varying Numbers of Oxygen Molecules. The O_2 adsorption energies of the optimized Cu and Ag−Cu bimetallic nanoparticles were calculated by varying the number of adsorbed O_2 molecules. Up to seven O_2 molecules were used to identify the adsorption trends. Among the 12 generated Ag−Cu bimetallic nanoparticles in Figure 4, the seventh configuration was chosen because it was the most stable. We considered four adsorption sites of hollow-top_1 (h-t_1), hollow-top_2 (h-t_2), hollow-top_3 (h-t_3), and bridge (b) in Figure 5a. The three h-t sites are almost the same in the middle of (111) with the only difference being the molecular orientation. The b site connects two metal atoms on the (111) edge. Calculation results indicate that the h-t sites were more stable than the b site, and the h-t_2 site was the most stable in both Cu monometallic and Ag−Cu bimetallic nanoparticles. Oxygen molecules were then added one by one as shown in Figure 5b,c. When oxygen molecules were placed on Cu, they were placed on the opposite side compared to the previously adsorbed one (see Figure 5b), while all the adsorption sites were confined to h-t_2 of Figure 5a. However, this rule could not be followed exactly for Ag−Cu bimetallic nanoparticles because oxygen is strongly adsorbed near the Cu atoms in all circumstances (see Figure 5c). Thus, all oxygen molecules were placed on Cu atoms that were as far away as possible from the previously adsorbed oxygen molecule.

The adsorption energy under each condition was calculated, and the results are shown in Figure 6. Second-order polynomial fitting highlights the adsorption trends for each nanoparticle. A negative value indicates that the O_2 molecules were adsorbed with larger energies corresponding to stronger adsorption or a more stable state. In contrast, a positive value indicates that O_2 molecules were difficult to adsorb. For the first O_2 molecule, the adsorption energy difference (approximately 0.225 eV) between the Cu and Ag−Cu bimetallic nanoparticles is not large. However, there are substantial differences (i.e., approximately 0.849 eV) in the adsorption energy for the last O_2 molecule. The reason for the weak adsorption energy on the Ag−Cu bimetallic nanoparticle arises from the difference in the redox potentials of Ag and Cu. Ag has a higher redox potential and can accept electrons from Cu. Thus, Cu atoms in the Ag−Cu bimetallic nanoparticles have lower electron densities compared to those in the Cu nanoparticles. Indeed, when we calculated the atomic charge of the Ag−Cu bimetallic nanoparticle using Mulliken charge analysis, the atomic charge

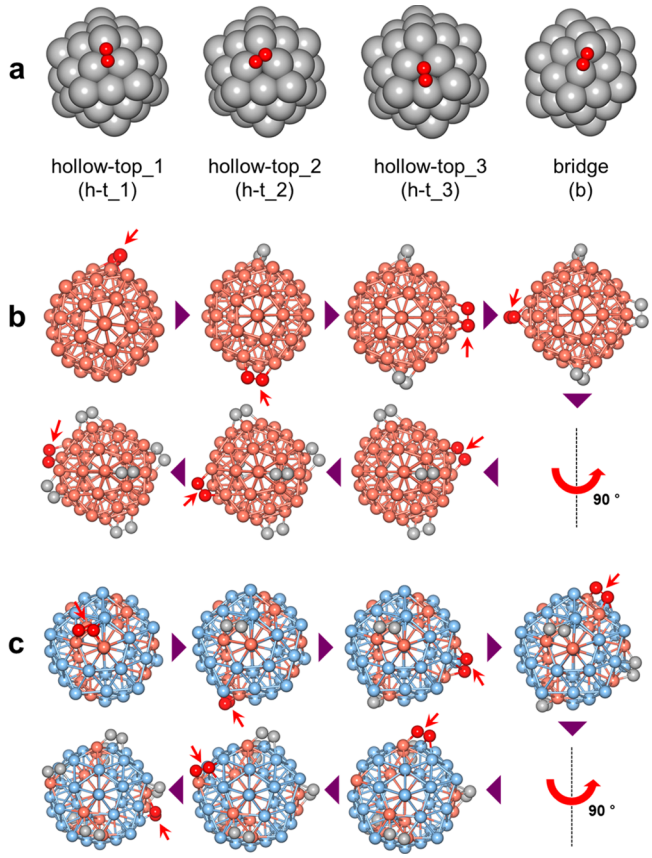

Figure 5. (a) Four adsorption sites for O_2. Stable adsorption site when we added O_2 one by one on the (b) Cu and (c) Ag−Cu bimetallic nanoparticle is presented. In each system, O_2 is added one by one on the nanoparticle by following arrows until the seventh O_2 is adsorbed. O_2 in red color means newly added O_2, and O_2 in gray color means already adsorbed O_2.

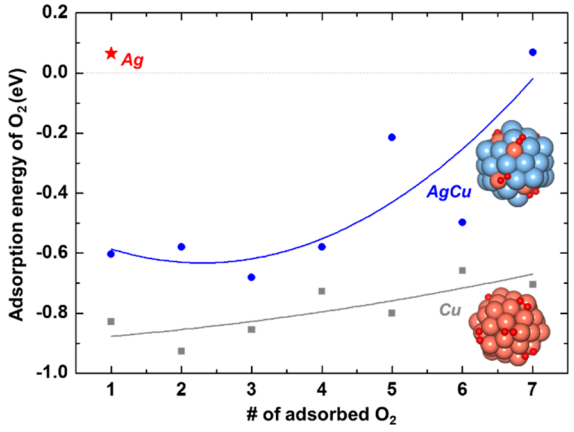

Figure 6. Adsorption energy of O_2 molecules on different nanoparticles. The gray squares represent the adsorption energies on the Cu nanoparticles; the blue circles represent the adsorption energies on the Ag−Cu bimetallic nanoparticles; and the red star represents the adsorption energies on the Ag nanoparticles.

of Cu in the Ag−Cu bimetallic nanoparticle had a positive value (+0.373 e).[59] This result strongly supports the electronic interaction between the Ag and Cu, which was assumed to explain the peak shift in the XPS from the experimental analysis.[18] The lower electron density makes Cu less active in bonding with the O_2 molecules. However, the Ag atoms that

dx.doi.org/10.1021/jp506069c | J. Phys. Chem. C 2014, 118, 26324−26331

accept electrons from Cu do not lead to a significant increase in the affinity to O_2 molecules because the electrons donated by the Cu atoms are diluted over a larger number of Ag atoms in the nanoparticle. Thus, the first O_2 adsorption energy on the Ag−Cu bimetallic nanoparticle is weaker than that on the Cu nanoparticle. The deficiency of electrons in the Cu becomes more severe when additional O_2 is adsorbed. As a result, the adsorption energy difference between the Ag−Cu bimetallic nanoparticle and the Cu nanoparticle rapidly increases. As shown in Figure 6, eventually, the adsorption energy of the seventh O_2 molecule on the Ag−Cu bimetallic nanoparticle is similar to that of the Ag nanoparticle. That is, the Ag−Cu bimetallic nanoparticle shows noble Ag nanoparticle-like characteristics when the seventh O_2 molecule is adsorbed. In addition, the adsorption energy of the seventh O_2 molecule on the Ag−Cu bimetallic nanoparticle has a positive value, which indicates an unstable or unfavorable state. The Ag−Cu bimetallic nanoparticle is more resistant to O_2 adsorption compared to the Cu nanoparticle because there is a smaller number of surface-exposed Cu atoms compared to the number of entire Cu atoms in this Ag−Cu bimetallic nanoparticle and electronic interaction between Ag and Cu atoms in the Ag−Cu bimetallic nanoparticle. This smaller number of surface-exposed Cu atoms can directly affect the adsorption energy of O_2 molecules because a smaller number of surface Cu atoms can accelerate deficiency of electrons in Cu atoms.

4. CONCLUSIONS

In summary, highly monodisperse Ag−Cu bimetallic nanoparticles were synthesized by sequential thermal decomposition and galvanic displacement reactions. Several independent experiments (HRTEM and cross-sectional EDS analysis) indicated randomly mixed shape of nanoparticles. XPS measurement showed that the Cu atoms of the Ag−Cu bimetallic nanoparticles were less oxidized than those in the Cu-only nanoparticles. To provide a deeper understanding of the oxidation resistance, computer simulations were conducted based on the experimental results. The calculated O_2 adsorption energy for the Ag−Cu 55-atom nanoparticle decreased dramatically as the numbers of adsorbed molecules increased, whereas the adsorption energy of the Cu 55-atom nanoparticle had a much weaker dependence on the number of O_2 molecules. This finding suggests that Ag−Cu bimetallic nanoparticles can solve the oxidation problem of Cu as well as the cost issue of Ag without the need for complex capping or reduction processes.

AUTHOR INFORMATION

Corresponding Author

*Tel.: +82 42 350 3334. Fax: +82 42 350 3310. E-mail: hmlee@kaist.ac.kr.

Notes

The authors declare no competing financial interest.

ACKNOWLEDGMENTS

This research was supported by the NLRL (National Leading Research Laboratory) program through the National Research Foundation of Korea (NRF) grant funded by the Korea government (MEST) (no. 2011-0028612). Prof. Moonsub Shim acknowledges the support of the Brain Pool program through the MSIP (Ministry of Science, ICT& Future Planning).

REFERENCES

(1) Jung, I.; Shin, K.; Kim, N. R.; Lee, H. M. Synthesis of Low-Temperature-Processable and Highly Conductive Ag Ink by a Simple Ligand Modification: the Role of Adsorption Energy. *J. Mater. Chem. C* **2013**, *1*, 1855−1862.

(2) Bell, A. T. The Impact of Nanoscience on Heterogeneous Catalysis. *Science* **2003**, *299*, 1688−1691.

(3) Kim, H. Y.; Lee, H. M.; Henkelman, G. CO Oxidation Mechanism on CeO_2-Supported Au Nanoparticles. *J. Am. Chem. Soc.* **2012**, *134*, 1560−1570.

(4) Jin, R.; Cao, Y. C.; Hao, E.; Métraux, G. S.; Schatz, G. C.; Mirkin, C. A. Controlling Anisotropic Nanoparticle Growth Through Plasmon Excitation. *Nature* **2003**, *425*, 487−490.

(5) Lu, A. H.; Salabas, E. L.; Schüth, F. Magnetic Nanoparticles: Synthesis, Protection, Functionalization, and Application. *Angew. Chem., Int. Ed.* **2007**, *46*, 1222−1244.

(6) Choi, C. S.; Jo, Y. H.; Kim, M. G.; Lee, H. M. Control of Chemical Kinetics for Sub-10 nm Cu Nanoparticles to Fabricate Highly Conductive Ink Below 150°C. *Nanotechnology* **2012**, *23*, 065601.

(7) Kim, D. H.; Shin, K.; Lee, H. M. CO Oxidation on Positively and Negatively Charged Ag_{13} Nanoparticles. *J. Phys. Chem. C* **2011**, *115*, 24771−24777.

(8) Kim, H. Y.; Han, S. S.; Ryu, J. H.; Lee, H. M. Balance in Adsorption Energy of Reactants Steers CO Oxidation Mechanism of Ag13 and Ag12Pd1 Nanoparticles: Association Mechanism versus Carbonate-Mediated Mechanism. *J. Phys. Chem. C* **2010**, *114*, 3156−3160.

(9) Shin, K.; Kim, D. H.; Lee, H. M. Catalytic Characteristics of AgCu Bimetallic Nanoparticles in the Oxygen Reduction Reaction. *ChemSusChem* **2013**, *6*, 1044−1049.

(10) Grouchko, M.; Kamyshny, A.; Magdassi, S. Formation of Air-Stable Copper-Silver Core-Shell Nanoparticles for Inkjet Printing. *J. Mater. Chem.* **2009**, *19*, 3057−3062.

(11) Kim, H. Y.; Kim, D. H.; Ryu, J. H.; Lee, H. M. Design of Robust and Reactive Nanoparticles with Atomic Precision: 13Ag-Ih and 12Ag−1X (X = Pd, Pt, Au, Ni, or Cu) Core−Shell Nanoparticles. *J. Phys. Chem. C* **2009**, *113*, 15559−15564.

(12) Shin, K.; Kim, D. H.; Yeo, S. C.; Lee, H. M. Structural Stability of AgCu Bimetallic Nanoparticles and Their Application as a Catalyst: A DFT Study. *Catal. Today* **2012**, *185*, 94−98.

(13) Muzikansky, A.; Nanikashvili, P.; Grinblat, J.; Zitoun, D. Ag Dewetting in Cu@Ag Monodisperse Core−Shell Nanoparticles. *J. Phys. Chem. C* **2013**, *117*, 3093−3100.

(14) Han, W.-S.; Hong, J.-M.; Kim, H.-S.; Song, Y.-W. Multi-Pulsed White Light Sintering of Printed Cu Nanoinks. *Nanotechnology* **2011**, *22*, 395705.

(15) Tsuji, M.; Hikino, S.; Tanabe, R.; Matsunaga, M.; Sano, Y. Syntheses of Ag/Cu Alloy and Ag/Cu Alloy Core Cu Shell Nanoparticles Using a Polyol Method. *CrystEngComm* **2010**, *12*, 3900−3908.

(16) Cushing, B. L.; Kolesnichenko, V. L.; O'Connor, C. J. Recent Advances in the Liquid-Phase Syntheses of Inorganic Nanoparticles. *Chem. Rev.* **2004**, *104*, 3893−3946.

(17) Park, J.; Joo, J.; Kwon, S. G.; Jang, Y.; Hyeon, T. Synthesis of Monodisperse Spherical Nanocrystals. *Angew. Chem., Int. Ed.* **2007**, *46*, 4630−4660.

(18) Chen, Z.; Mochizuki, D.; Maitani, M. M.; Wada, Y. Facile Synthesis of Bimetallic Cu−Ag Nanoparticles Under Microwave Irradiation and Their Oxidation Resistance. *Nanotechnology* **2013**, *24*, 265602.

(19) Hiramatsu, H.; Osterloh, F. E. A Simple Large-Scale Synthesis of Nearly Monodisperse Gold and Silver Nanoparticles With Adjustable Sizes and With Exchangeable Surfactants. *Chem. Mater.* **2004**, *16*, 2509−2511.

(20) Lin, X. Z.; Teng, X.; Yang, H. Direct Synthesis of Narrowly Dispersed Silver Nanoparticles Using a Single-Source Precursor. *Langmuir* **2003**, *19*, 10081−10085.

(21) Rifkin, J. xmd.sourceforge.net; The Center for Simulations, University of Connecticut (accessed 10/24/2014).
(22) Qi, Y.; Ikeda, H.; Cagin, T.; Samwer, K.; Johnson, W. L.; Goddard, W. A., III. Deformation Behavior of FCC Crystalline Metallic Nanowires Under High Strain Rates. *MRS Online Proc. Libr.* **1998**, *554*, 367−372.
(23) Kim, H. Y.; Kim, H. G.; Kim, D. H.; Lee, H. M. Overstabilization of the Metastable Structure of Isolated Ag−Pd Bimetallic Clusters. *J. Phys. Chem. C* **2008**, *112*, 17138−17142.
(24) Sutton, A. P.; Chen, J. Long-Range Finnis-Sinclair Potentials. *Philos. Mag. Lett.* **1990**, *61*, 139−146.
(25) vKim, H. Y.; Kim, H. G.; Ryu, J. H.; Lee, H. M. Preferential Segregation of Pd Atoms in the Ag-Pd Bimetallic Cluster: Density Functional Theory and Molecular Dynamics Simulation. *Phys. Rev. B* **2007**, *75*, 212105.
(26) Gear, C. W. *Numerical Initial Value Problems in Ordinary Differential Equations*; Prentice Hall: Englewood Cliffs, New Jersey, USA, 1971.
(27) Delley, B. From Molecules to Solids With the DMol^3 Approach. *J. Chem. Phys.* **2000**, *113*, 7756−7764.
(28) Delley, B. DMol^3 DFT Studies: From Molecules and Molecular Environments to Surfac es and Solids. *Comput. Mater. Sci.* **2000**, *17*, 122−126.
(29) Perdew, J. P.; Wang, Y. Accurate and Simple Analytic Representation of the Electron-Gas Correlation Energy. *Phys. Rev. B* **1992**, *45*, 13244−13249.
(30) Perdew, J. P.; Burke, K.; Ernzerhof, M. Generalized Gradient Approximation Made Simple. *Phys. Rev. Lett.* **1996**, *77*, 3865−3868.
(31) Perdew, J. P.; Burke, K.; Ernzerhof, M. Generalized Gradient Approximation Made Simple [Phys. Rev. Lett. 77, 3865 (1996)]. *Phys. Rev. Lett.* **1997**, *78*, 1396.
(32) Zhang, Y.; Yang, W. Comment on "Generalized Gradient Approximation Made Simple. *Phys. Rev. Lett.* **1998**, *80*, 890.
(33) vHammer, B.; Hansen, L. B.; Nørskov, J. K. Improved Adsorption Energetics Within Density-Functional Theory Using Revised Perdew-Burke-Ernzerhof Functionals. *Phys. Rev. B* **1999**, *59*, 7413.
(34) Nørskov, J. K.; Rossmeisl, J.; Logadottir, A.; Lindqvist, L.; Kitchin, J. R.; Bligaard, T.; Jonsson, H. Origin of the Overpotential for Oxygen Reduction at a Fuel-Cell Cathode. *J. Phys. Chem. B* **2004**, *108*, 17886−17892.
(35) Falsig, H.; Hvolbæk, B.; Kristensen, I. S.; Jiang, T.; Bligaard, T.; Christensen, C. H.; Nørskov, J. K. Trends in the Catalytic CO Oxidation Activity of Nanoparticles. *Angew. Chem., Int. Ed.* **2008**, *120*, 4913−4917.
(36) Pogodin, S.; López, N. A More Accurate Kinetic Monte Carlo Approach to a Monodimensional Surface Reaction: The Interaction of Oxygen with the RuO_2(110) Surface. *ACS Catal.* **2014**, *4*, 2328−2332.
(37) Delley, B. Hardness Conserving Semilocal Pseudopotentials. *Phys. Rev. B* **2002**, *66*, 155125.
(38) Baletto, F.; Ferrando, R. Structural Properties of Nanoclusters: Energetic, Thermodynamic, and Kinetic Effects. *Rev. Mod. Phys.* **2005**, *77*, 371−423.
(39) Rapallo, A.; Rossi, G.; Ferrando, R.; Fortunelli, A.; Curley, B. C.; Lloyd, L. D.; Tarbuck, G. M.; Johnston, R. L. Global Optimization of Bimetallic Cluster Structures. I. Size-Mismatched Ag−Cu, Ag−Ni, and Au−Cu Systems. *J. Chem. Phys.* **2005**, *122*, 194308.
(40) Rossi, G.; Rapallo, A.; Mottet, C.; Fortunelli, A.; Baletto, F.; Ferrando, R. Magic Polyicosahedral Core-Shell Clusters. *Phys. Rev. Lett.* **2004**, *93*, 105503.
(41) Darby, S.; Mortimer-Jones, T. V.; Johnston, R. L.; Roberts, C. Theoretical Study of Cu−Au Nanoalloy Clusters Using a Genetic Algorithm. *J. Chem. Phys.* **2002**, *116*, 1536−1550.
(42) Barcaro, G.; Fortunelli, A.; Rossi, G.; Nita, F.; Ferrando, R. Electronic and Structural Shell Closure in AgCu and AuCu Nanoclusters. *J. Phys. Chem. B* **2006**, *110*, 23197−23203.
(43) Chen, M.; Feng, Y.-G.; Wang, X.; Li, T.-C.; Zhang, J.-Y.; Qian, D.-J. Silver Nanoparticles Capped by Oleylamine: Formation, Growth, and Self-Organization. *Langmuir* **2007**, *23*, 5296−5304.
(44) Hong, Z.-S.; Cao, Y.; Deng, J.-F. A Convenient Alcohothermal Approach for Low Temperature Synthesis of CuO Nanoparticles. *Mater. Lett.* **2002**, *52*, 34−38.
(45) Jeong, S.; Woo, K.; Kim, D.; Lim, S.; Kim, J. S.; Shin, H.; Xia, Y.; Moon, J. Controlling the Thickness of the Surface Oxide Layer on Cu Nanoparticles for the Fabrication of Conductive Structures by Ink-Jet Printing. *Adv. Funct. Mater.* **2008**, *18*, 679−686.
(46) Chen, L. Y.; Zhang, L.; Fujita, T.; Chen, M. W. Surface-Enhanced Raman Scattering of Silver@Nanoporous Copper Core−Shell Composites Synthesized by an In Situ Sacrificial Template Approach. *J. Phys. Chem. C* **2009**, *113*, 14195−14199.
(47) Yang, Y.; Liu, J.; Fu, Z.-W.; Qin, D. Galvanic Replacement-Free Deposition of Au on Ag for Core−Shell Nanocubes with Enhanced Chemical Stability and SERS Activity. *J. Am. Chem. Soc.* **2014**, *136*, 8153−8156.
(48) Gao, C.; Hu, Y.; Wang, M.; Chi, M.; Yin, Y. Fully Alloyed Ag/Au Nanospheres: Combining the Plasmonic Property of Ag with the Stability of Au. *J. Am. Chem. Soc.* **2014**, *136*, 7474−7479.
(49) Mekhalif, Z.; Fonder, G.; Laffineur, F.; Delhalle, J. Comparative Assessment of N-Dodecanethiol and N-Dodecaneselenol Monolayers on Electroplated Copper. *J. Electroanal. Chem.* **2008**, *621*, 245−253.
(50) Johansson, B.; Mårtensson, N. Core-Level Binding-Energy Shifts for the Metallic Elements. *Phys. Rev. B* **1980**, *21*, 4427−4457.
(51) Ghijsen, J.; Tjeng, L. H.; van Elp, J.; Eskes, H.; Westerink, J.; Sawatzky, G. A.; Czyzyk, M. T. Electronic Structure of Cu_2O and CuO. *Phys. Rev. B* **1988**, *38*, 11322−11330.
(52) Moulder, J. F.; Stickle, W. F. S.; Peter, E.; Sobol, P. E.; Bomben, K. D. *Handbook of X Ray Photoelectron Spectroscopy: A Reference Book of Standard Spectra for Identification and Interpretation of XPS Data*; Physical Electronics Inc.: Minnesota, USA, 1992.
(53) Kang, M.; Park, E. D.; Kim, J. M.; Yie, J. E. Manganese Oxide Catalysts for NO_x Reduction With NH_3 at Low Temperatures. *Appl. Catal., A* **2007**, *327*, 261−269.
(54) Sun, L.; Yan, F.; Zhang, H.; Wang, J.; Zeng, Y.; Wang, G.; Li, J. Strong Room-Temperature Ferromagnetism in Cu-Implanted Non-polar GaN Films. *J. Appl. Phys.* **2009**, *106*, 113921−4.
(55) Di Castro, V.; Furlani, C.; Gargano, M.; Ravasio, N.; Rossi, M. XPS Study of Copper Dispersion in CuO/Al_2O_3 Catalysts. *J. Electron Spectrosc. Relat. Phenom.* **1990**, *52*, 415−422.
(56) Xiaoyuan, J.; Liping, L.; Yingxu, C.; Xiaoming, Z. Effects of CuO/CeO_2 and CuO/γ-Al_2O_3 Catalysts on NO + CO Reaction. *J. Mol. Catal. A: Chem.* **2003**, *197*, 193−205.
(57) Doye, J. P. K.; Wales, D. J. Structural Consequences of the Range of the Interatomic Potential a Menagerie of Clusters. *J. Chem. Soc., Faraday Trans.* **1997**, *93*, 4233−4243.
(58) Tyson, W. R.; Miller, W. A. Surface Free Energies of Solid Metals: Estimation From Liquid Surface Tension Measurements. *Surf. Sci.* **1977**, *62*, 267−276.
(59) Mulliken, R. S. Electronic Population Analysis on LCAO-MO Molecular Wave Functions. I. *J. Chem. Phys.* **1955**, *23*, 1833−1840.